Title
CT-like MRI: a qualitative assessment of ZTE sequences for knee osseous abnormalities.

Journal
Skeletal Radiology: journal of radiology, pathology and orthopedics, 51(8)

Authors
Coy, Adam
Motamedi, Daria
Sun, Dong
et al.

Publication Date
2022-08-01

DOI
10.1007/s00256-021-03987-2

Peer reviewed

HHS Public Access

Author manuscript

Skeletal Radiol. Author manuscript; available in PMC 2023 August 01.

Published in final edited form as:

Skeletal Radiol. 2022 August ; 51(8): 1585–1594. doi:10.1007/s00256-021-03987-2.

CT-like MRI: a qualitative assessment of ZTE sequences for knee osseous abnormalities

Upasana Upadhyay Bharadwaj[1,*], **Adam Coy**[1,2], **Daria Motamedi**[1], **Dong Sun**[1,3], **Gabby B. Joseph**[1], **Roland Krug**[1], **Thomas M. Link**[1]

[1]Musculoskeletal Imaging, Department of Radiology and Biomedical Imaging, University of California San Francisco, 185 Berry Street, Suite 350, San Francisco, CA, 94107, USA

[2]Musculoskeletal Radiology, Vision Radiology, Dallas, TX, USA

[3]Department of Radiology, Tongji Hospital, Tongji Medical College, Huazhong University of Science and Technology, Wuhan, China

Abstract

Objective—To qualitatively evaluate the utility of zero echo-time (ZTE) MRI sequences in identifying osseous findings and to compare ZTE with optimized spoiled gradient echo (SPGR) sequences in detecting knee osseous abnormalities.

Materials and methods—ZTE and standard knee MRI sequences were acquired at 3T in 100 consecutive patients. Three radiologists rated confidence in evaluating osseous abnormalities and image quality on a 5-grade Likert scale in ZTE compared to standard sequences. In a subset of knees ($n = 57$) SPGR sequences were also obtained, and diagnostic confidence in identifying osseous structures was assessed, comparing ZTE and SPGR sequences. Statistical significance of using ZTE over SPGR was characterized with a paired t-test.

Results—Image quality of the ZTE sequences was rated high by all reviewers with 278 out of 299 (100 studies, 3 radiologists) scores ≥ 4 on the Likert scale. Diagnostic confidence in using ZTE sequences was rated “definitely certain” in 97%, 85%, 71%, and 73% of the cases for osteophytosis, subchondral cysts, fractures, and soft tissue calcifications/ossifications, respectively. In 74% of cases with osseous findings, reviewer scores indicated confidence levels (score ≥ 3) that ZTE sequences improved diagnostic certainty over standard sequences. The diagnostic confidence in using ZTE over SPGR sequences for osseous structures as well as abnormalities was favorable and statistically significant ($p < 0.01$).

*Corresponding author: Upasana.Bharadwaj@ucsf.edu.

Declarations

Conflict of interest

The authors no competing interests.

Conclusion—Incorporating ZTE sequences in the standard knee MRI protocol was technically feasible and improved diagnostic confidence for osseous findings in relation to standard MR sequences. In comparison to SPGR sequences, ZTE improved assessment of osseous abnormalities.

Keywords

Magnetic resonance imaging/methods; Knee; Knee joint; Diagnostic imaging; Bone diseases

Introduction

While musculoskeletal structures such as cartilage, ligaments, menisci, bone marrow, and muscles are primarily evaluated using MRI, cortical bone is not well-visualized with standard fast spin echo sequences (FSE) due to very short relaxation times of the mineralized bone and low water content. Muscle, fat, and other soft tissue T2/T2* relaxation times vary between 30 and 200 ms [1], whereas cortical bone has T2/T2* relaxation times of approximately 0.4 ms [2–9].

Zero echo time (ZTE) MR sequences use echo times as low as 0.1 ms [5, 8], enabling the acquisition of signal from structures with very short T2 relaxation properties such as the cortical bone. ZTE is acquired by rapidly switching between transmit and receive modes, which may introduce some sampling artifacts that include blurring and shadow artifacts, which can be subsequently corrected with sophisticated reconstruction algorithms as previously described [5]. CT-like visualization of bone from a ZTE acquisition is obtained with post-processing that includes inverse rescaling [6, 10]. To our knowledge, very few studies have established the utility of ZTE in knee imaging [11].

ZTE sequences with high fidelity reconstructions to visualize osseous abnormalities may be relevant in clinical practice, and several studies have investigated potential applications. Previous research has demonstrated the advantages of ZTE in evaluating osseous pathologies of the hip, shoulder, and cervical spine [12–14] as well as various applications in neuroradiology [15–17]. These studies concluded that there is strong agreement in relevant quantitative measurements as well as qualitative assessment comparing ZTE and CT, implying that ZTE may eventually become an alternative to CT imaging and thus minimize patient exposure to ionizing radiation.

Osseous structures can be visualized on other MRI sequences as well, with varying levels of granularity. Spoiled gradient recalled acquisition (SPGR) is a gradient echo sequence which spoils the transverse steady state by randomizing the phase of the Radiofrequency (RF) pulse, resulting in predominantly T1 contrast [18]. SPGR can also be inverted for CT-like visualization and has been effective in imaging trabecular bone, with prior studies establishing its utility in demonstrating bone architecture [19–21]. To our knowledge, ZTE and SPGR sequences so far have not been compared concerning visualization of bony structures.

Thus, the purpose of this prospective study was to evaluate the utility and performance of ZTE MRI in identifying knee osseous findings in relation to standard MR sequences and to compare ZTE with optimized SPGR sequences in detecting knee osseous abnormalities.

Materials and methods

Study design

This Health Insurance Portability and Accountability Act (HIPAA) compliant prospective study was approved by our institution's committee on human research with informed consent being waived. This multi-reader study evaluated the image quality and clinical usefulness of ZTE and SPGR sequences in addition to standard MRI sequences in patients undergoing a non-contrast MRI of the knee. The study is based on the assessment of various qualitative attributes, such as image quality and reviewers' confidence in ZTE sequences for diagnosing osseous abnormalities using Likert scales.

Patient cohort

We included 100 consecutive patients who had MRI scans of the knee performed with a standard clinical MRI protocol and an additional ZTE sequence. In a subset of patients (n = 57), an additional bone optimized SPGR sequence was also acquired. Clinical indications for the MRI in these patients included pain (n = 35), suspected internal derangement of knee (n = 28), trauma (n = 23), and evaluation of post-operative changes (n = 14).

Image acquisition

All MRI studies were acquired with a 3T MRI scanner (Discovery MR750 scanner, GE Healthcare, Waukesha, Wisconsin) and a 16-channel flex medium coil (Neocoil, Pewaukee, Wisconsin). Standard knee sequences included sagittal intermediate weighted fat-saturated (Iw-FS) and proton-density (PD) weighted 2D fast spin echo (FSE) sequences, axial, and coronal Iw-FS 2D FSE sequences as well as T1-weighted coronal 2D FSE sequences. In addition, sagittal 3D ZTE and SPGR sequences were included in the protocol. Both sequences were optimized to maximize contrast between bone and soft tissue within similar scan times and inverted for CT-like visualization. ZTE sequences were acquired in all 100 patients while SPGR acquired in a subset of 57 patients. The imaging protocols and pertinent imaging parameters are presented in Table 1.

Image analysis

ZTE, SPGR, and routine MRI sequences were analyzed independently by three musculoskeletal (MSK) fellowship trained radiologists with 23, 8, and 5 years of experience on standard PACS workstations (Agfa, Mortsel, Belgium) without time constraints and ambient background lighting. Image quality, diagnostic utility, impact on patient management, and differences in image quality between ZTE and SPGR sequences were graded by each radiologist, who reviewed all images.

Ratings were performed on *image quality* attributes that included image artifact, image motion, tissue contrast, sharpness of contrast, delineation of cortical bone, and delineation of trabecular bone. These attributes were selected as the most pertinent metrics for assessing

the quality of an image for evaluating osseous findings; they were rated qualitatively by three board certified radiologists. Prior to review, a training session was performed where the radiologists rated a subset of 10 cases together for calibration purposes.

A 5-grade Likert scale was used spanning “very good” (unimpaired depiction of all structures), “good” (minimal impairment of image, but preservation of all structural detail), “adequate” (impaired depiction of small areas), “poor” (substantial obscuration of structures), and “very poor” (complete obscuration of structures).

Reviewers also evaluated the studies concerning *osseous abnormalities* including cortical, subcortical, and avulsion fractures, calcified and ossified bodies, subchondral cysts, osteophytes, osteolysis, and other osseous deformities. The reviewers rated their confidence in identifying these osseous abnormalities using a 5-grade Likert scale differentiating “definitely visualized” (osseous abnormalities clearly delineated and well shown), “probably visualized” (osseous structures appear to be shown but are not well-delineated), “uncertain” (unclear delineation of osseous abnormality), probably not visualized” (abnormality likely not shown but bony structures are not well-delineated), and “definitely not visualized” (osseous abnormality definitely not shown).

The utility of ZTE was further assessed qualitatively for overall impact in three categories: alters patient management, increases diagnostic confidence, and may provide additional value to the patient. These attributes were graded on a 5-grade Likert scale spanning “definitely certain”, “certain”, “probable diagnosis”, “probably not”, and “definitely not.”

In patients who had both ZTE and SPGR sequences, the two sequences were compared side by side for evaluation of osseous structures, assessing whether soft tissues limited evaluation of osseous structures and whether osseous structures were visualized better on the ZTE sequence than on SPGR. Two additional attributes – “diagnostic confidence of bony abnormalities using ZTE” and “bony abnormalities seen better on ZTE than on SPGR” – were also evaluated on the subset of patients in whom both ZTE and SPGR sequences were acquired. The grading was performed using a 5-grade Likert scale: “definitely certain” (ZTE is definitely better than SPGR for visualizing bony abnormalities), certain, probably certain, not certain, and definitely not certain (ZTE is definitely not better in the evaluation of bony abnormalities than SPGR).

Statistical analysis

The Likert scores used to assess image quality of ZTE were analyzed using histograms to evaluate the distribution of scores ranging from “unimpaired depiction of all structures” and “complete obscuration of images” for the following image quality attributes: contrast, sharpness, artifact, motion, cortical bone depiction, and trabecular bone depiction. Similarly, Likert scores used to assess the diagnostic confidence of ZTE were analyzed with histograms to determine the distribution of scores ranging from “definitely certain” to “definitely not certain.” Statistical significance of diagnostic confidence (using Likert scores) of ZTE over SPGR for osseous abnormalities was evaluated using a paired t-test [22] (p-value threshold of 0.05 selected *a priori*) for two related attributes from the study: (a) bony structures better seen on ZTE than on SPGR (b) soft tissue limits evaluation of osseous

structures on SPGR. The qualitative attributes along with their corresponding Likert scores were also assessed for consistency and reproducibility with pairwise inter-reader agreement scores computed between all three reviewers using the Cohen's kappa statistic. A kappa score of 0.2 or higher was considered fair agreement, 0.4 or higher was considered moderate agreement, and 0.6 or higher was considered substantial [23]. The SciPy v1.6.0 python library and its stats module were used for all statistical analyses reported in this paper [24].

Results

Patient cohort

The patient cohort ($n = 100$) consisted of forty-four female and fifty-six male patients with an average age of 40.0 +/− 16.1 years. The average BMI and standard deviation were 26.3 +/− 4.6 kg/m^2. The patients were noted to have a range of osseous abnormalities including cortical, subcortical, and avulsion fractures, calcified and ossified bodies, subchondral cysts, osteophytes, osteolysis, and other osseous deformities.

Image quality of ZTE sequences

A total of 299 grades were used in the analysis, instead of 300 (100 studies × 3 reviewers) since one patient was graded by only two of the three reviewers. ZTE image quality was rated high by all reviewers with 93.0% (278 of 299) scores ≥ 4 on the Likert scale across various image quality attributes such as contrast, sharpness, artifact, motion, and cortical bone depiction. In the case of image artifact and motion, unimpaired depiction of all structures (score = 5) was observed in 72.6% (217 of 299) and 91.3% (273 of 299) of the grades, respectively. With the notable exception of trabecular bone depiction, in which 61.5% (184 of 299) of the scores indicated substantial or complete obscuration of the structure (grade 1 and 2), ZTE image quality was graded high. The relative percentages as well as absolute counts for each feature are summarized in Table 2.

ZTE vs. standard sequences for evaluating osseous structures and abnormalities

ZTE sequences were observed to be favorable overall for assessing osseous structures and diagnosing osseous abnormalities. The graded osseous abnormalities include osteophytosis (104 of 299), subchondral cysts (47 of 299), soft tissue calcifications (26 of 299), and fractures (45 of 299). In some patients, more than one osseous abnormality are visualized and graded (i.e., the findings are not mutually exclusive). Quantitatively, 97.1% (101 of 104) of the grades had a score = 5 (definitely visualized) for confidence in assessing osteophytosis using ZTE; 85.1% (40 of 47) of the grades had a score = 5 for confidence in assessing subchondral cysts; 73.0% (19 of 26) of the grades had a score=5 for confidence in assessing soft tissue calcifications; and 71.1% (32 of 45) of the grades had a score = 5 for confidence in assessing fractures. The distribution of Likert scores across all osseous structures is presented in Table 3, indicating strong confidence in using ZTE for assessing osseous structures. Figure 1 shows a representative ZTE image with osteophytes substantially better visualized than on standard FSE sequences. Figure 2 demonstrates that ZTE sequences can also show bony abnormalities adjacent to metal in a patient with ACL reconstruction. Figure 3 shows that osteochondral bodies posterior to the tibia are

well-characterized on ZTE as well as SPGR, but not well-visualized on the standard clinical sequences.

In 74.4% (180 of 242) of cases with osseous findings, reviewer scores indicated confidence levels (score ≥ 3) that ZTE improved diagnostic certainty, compared to 58.6% (34 of 58) of the cases without osseous findings that were rated ≥ 3 for improved diagnostic certainty. In 53.7% (130 of 242) of cases with osseous findings, reviewers indicated that ZTE could alter patient management (score ≥ 3), versus 41.4% (24 of 58) of the cases without osseous findings. In 69.8% (169 of 242) of cases with osseous findings, reviewer scores indicated high confidence (score ≥ 3) that ZTE would provide additional value to the patient. Table 4 presents the distribution of scores across all three categories for osseous findings (n = 242) and Table 5 presents the distribution of scores across all three categories for cases without osseous findings (n = 58). Figure 4 demonstrates a fracture which is better seen with the ZTE sequence compared with standard FSE sequences which only show bone marrow edema pattern.

ZTE vs. SPGR sequences for evaluating osseous structures and abnormalities

The diagnostic confidence in using ZTE over SPGR for osseous structures was favorable and statistically significant with a mean and standard deviation Likert scores of 3.08 +/− 1.65 for ZTE and 2.59 +/− 1.60 for SPGR sequences ($p < 0.01$). The diagnostic confidence in using ZTE over SPGR for osseous abnormalities was also favorable and statistically significant with a mean and standard deviation Likert scores of 4.38 +/− 0.83 for ZTE and 2.59 +/− 1.60 for SPGR sequences ($p < 0.01$). Table 6 presents the distribution of scores for three attributes of the study: “bony structures better seen on ZTE than on SPGR”, “bony abnormalities better seen on ZTE than on SPGR”, and “soft tissue limits evaluation of osseous structures on SPGR”. Figure 5 shows that ZTE sequences were superior to SPGR sequences in demonstrating osteophytes, which are not well-differentiated from adjacent soft tissues in the SPGR sequence. The same is seen for osteochondral bodies which are better visualized with ZTE sequences compared to SPGR sequences as demonstrated in Fig. 3, where it is more difficult to separate osteochondral bodies from adjacent soft tissues in the SPGR image. Fractures, however, are shown similarly well with both ZTE and SPGR sequences as shown in Fig. 6, where the patellar fracture is well-visualized on both ZTE and SPGR sequences. It was also noted that the trabecular bone architecture was better seen on the SPGR sequences.

Reproducibility

Inter-rater agreement was moderate with pairwise Cohen’s kappa scores (reviewer 1/reviewer 2, reviewer 2/reviewer 3, reviewer 3/reviewer 1) of (0.41, 0.52, 0.58) for Likert scores assessing confidence in diagnosing osteophytosis using ZTE; and (0.43, 0.55, 0.58) for scores assessing confidence in diagnosing subchondral cysts. The agreement was fair in more subjective categories such as Likert scores assessing whether *bony structures* were better visualized on ZTE compared to SPGR sequences with agreements of (0.57, 0.28, 0.31) and agreements of (0.63, 0.28, 0.27) for Likert scores assessing whether *bony abnormalities* were better visualized on ZTE compared to SPGR sequences. The pairwise kappa agreement scores are reported in Table 7.

Discussion

In this prospective study, we qualitatively evaluated the utility of ZTE MR sequences in identifying knee osseous findings and compared ZTE with an optimized SPGR sequence in detecting knee osseous abnormalities. Likert scale type assessment was performed which is based on subjective, qualitative evaluation, which is not strictly quantitative, but an accepted method to score the value of radiologic imaging techniques. We found strong consensus among the reviewers that ZTE may be a valuable addition to MR-based visualization of osseous findings in the knee. The *image quality* of ZTE was overall rated high by three radiologists and favorable for assessing osseous structures. We found ZTE sequences to be a useful addition to standard routine knee protocols, providing pertinent information on osseous abnormalities. ZTE also improved diagnostic certainty, with increased confidence in using ZTE over SPGR for diagnosing osseous abnormalities.

While previous studies have analyzed the value of ZTE sequences at other anatomical sites, the novelty of our study is in analyzing the knee joint ZTE imaging by three board-certified radiologists and comparing ZTE and SPGR sequences concerning their performance in visualizing bony structures. To the best of our knowledge, this is one of the first studies to evaluate ZTE sequences for diagnosing knee osseous abnormalities and directly compare ZTE and SPGR sequences. Recent studies in the hip [13] and shoulder [14] have thoroughly assessed ZTE in comparison with CT across various quantitative metrics as well as qualitative features used in clinical practice. They established the utility of ZTE sequences as an alternative to CT imaging with strong inter-group agreement statistics between ZTE sequences and CT. Our study was focused entirely on qualitative attributes measured using Likert scales ranging from image quality to diagnostic confidence, assessed by three board-certified radiologists. Prior studies have established the value of ZTE in clinical practice; a natural next step is to assess how ZTE might compare with other CT-like MRI sequences.

A key aspect of our study therefore included comparison of ZTE and SPGR sequences. SPGR sequences were previously optimized and used for the imaging of trabecular bone architecture [19–21, 25, 26], thus motivating a direct comparison between ZTE, SPGR, and standard MR sequences acquired as per the clinical protocol. Our results indicate that osseous findings are well-visualized on ZTE sequences compared to standard sequences as shown in select examples; in most cases, osseous abnormalities were also better seen on ZTE compared to SPGR sequences, with the notable exception of trabecular bone, where the SPGR sequence appeared superior compared to the ZTE sequence – albeit prior studies have indicated that the trabecular bone can be also visualized on ZTE sequences [6, 8].

Including ZTE as an additional sequence introduces approximately four minutes to standard MRI protocols, which appears justified given the benefits of visualizing osseous structures with better diagnostic confidence compared to standard MR protocols. Incorporating ZTE sequences may potentially mitigate the need for additional imaging such as CT to assess osseous abnormalities. While our study could not include CT as an additional scan, a detailed evaluation of clinically relevant quantitative metrics of hip morphology showed significant agreement of angular measurements, with inter-modal correlation as high as 0.9

between CT and ZTE MRI [13]. Similar trends have been observed in imaging of the shoulder [27]. A recent study assessing 3D CT vs ZTE sequences for measuring the width of the glenoid bone reported a mean-difference of 0.5 mm between the two modalities, indicating strong agreement [27]. An earlier study showed high inter-modal correlations of 0.7, within the same range as inter-rater correlations, across quantitative measures spanning glenoid vault depth, version angle, and best-fit circle diameter [14]. Overall, prior studies demonstrate strong CT-like outcomes across knee, shoulder, and hip scans depending on ZTE acquisition parameters and imaging techniques such as long-T2 suppression [28, 29].

ZTE sequences therefore could be clinically useful in knee applications such as surgical planning of patient-specific instrumentation to assess whether arthroplasty may be indicated, with MRI as virtual CT for volumetric reconstructions of bone [30]. ZTE sequences may also provide improved visualization of associated bony injuries after an ACL tear such as avulsion injuries of the lateral tibial plateau (Segond fractures) or tibial plateau depression fractures. Differentiation between a non-displaced fracture and an osseous contusion can be difficult on standard MRI sequences due to low signal of the bone cortex [11], and with improved visualization of the osseous cortex, ZTE sequences may potentially improve detection of fractures [13, 14, 27, 31].

Given the broad implications of CT-like MRI, synthesis of a virtual CT from MRI has been of significant interest in the machine learning community. A recent study showed that synthetic CT can be constructed within 65 Hounsfield units of the original CT entirely from T2-weighted MRI [32]. A comparison of various gradient echo-based MR images further concluded that Dixon-styled fat suppression was more effective for MR-to-CT synthesis compared to other sequences [33]. While these methods are nascent and largely algorithmic, we suspect that introducing ZTE MRI, which is amenable to high fidelity bone imaging, may be a promising avenue for generating more accurate, visually similar synthetic CT from MRI.

As indicated earlier, a key limitation of our study is that we did not include CT imaging for direct comparison of osseous abnormalities to further strengthen our assertions; our study included 100 consecutive patients in whom a CT scan was not acquired as part of the clinical protocol (e.g., atraumatic knee pain, osteoarthritis, sports injuries, post-operative knee). Please note, however, that previous studies compared ZTE sequences and CT studies with favorable results [13, 14, 27, 34]. A second limitation of our study is that SPGR sequences were not acquired in all 100 patients, but given that this study was performed in a clinical setting, it was not possible to add both sequences to the standard protocol in all patients. Lastly, while high confidence visualization of osseous abnormalities using ZTE is not perfect (e.g., 71% of cases with high confidence for fracture detection), subsequent improvement of the sequences and research efforts in acquisition may bridge the gap. While cortical bone is well-visualized with current sequences, ZTE sequences have limitations in visualizing trabecular bone. Improving ZTE sequences to also better visualize trabecular bone is work in progress; artificial intelligence algorithms have been developed that may address these issues in the future [35], and we believe that our study identifies imperfect visualization of trabecular bone with current ZTE sequences as an important avenue for future research.

In conclusion, incorporating ZTE MRI sequences in the standard knee imaging protocol is technically feasible and improves diagnostic confidence for osseous abnormalities compared to standard MRI sequences, resulting in a more comprehensive assessment of the knee, in particular as concerns assessment of loose bodies, fractures, and bony deformities. ZTE sequences were also superior to SPGR sequences in evaluating bony abnormalities and may be a useful adjunct to assess bony abnormalities.

References

1. Gold GE, Han E, Stainsby J, Wright G, Brittan J, Beaulieu C. Musculoskeletal MRI at 3.0 T: relaxation times and image contrast. AJR Am J Roentgenol 2004; 183:343–351. [PubMed: 15269023]
2. Du J, Bydder GM. Qualitative and quantitative ultrashort-TE MRI of cortical bone. NMR Biomed 2012; 26(5):489–506. [PubMed: 23280581]
3. Du J, Carl M, Bydder M, Takahashi A, Chung CB, Bydder GM. Qualitative and quantitative ultrashort echo time (UTE) imaging of cortical bone. J Magn Reson 2010; 207(2):304–311. [PubMed: 20980179]
4. Krug R, Larson PEZ, Wang C, Burghardt AJ, Kelley DAC, Link TM, et al. Ultrashort echo time MRI of cortical bone at 7 tesla field strength: a feasibility study. J Magn Reson Imaging 2011; 34(3):691–695. [PubMed: 21769960]
5. Larson PEZ, Han M, Krug R, Jakary A, Nelson SJ, Vigneron DB, et al. Ultrashort echo time and zero echo time MRI at 7T. MAGMA 2016; 29(3):359–370. [PubMed: 26702940]
6. Ma Y-J, Jerban S, Jang H, Chang D, Chang EY, Du J. Quantitative ultrashort echo time (UTE) magnetic resonance imaging of bone: an update. Front Endocrinol (Lausanne) 2020; 11.
7. Reichert ILH, Robson MD, Gatehouse PD, He T, Chappell KE, Holmes J, et al. Magnetic resonance imaging of cortical bone with ultrashort TE pulse sequences. Magn Reson Imaging 2005; 23(5):611–618. [PubMed: 16051035]
8. Weiger M, Stampanoni M, Pruessmann KP. Direct depiction of bone microstructure using MRI with zero echo time. Bone 2013; 54(1):44–47. [PubMed: 23356986]
9. Abbasi-Rad S, Rad HS. Quantification of human cortical bone bound and free water in vivo with ultrashort echo time MR imaging: a model-based approach. Radiology 2017; 283(3):862–872. [PubMed: 28051911]
10. Stillwater L, Koenig J, Maycher B, Davidson M. 3D-MR vs. 3D-CT of the shoulder in patients with glenohumeral instability. Skeletal Radiol 2017; 46(3):325–331. [PubMed: 28028575]
11. Mohankumar R, White LM, Naraghi A. Pitfalls and pearls in MRI of the knee. AJR Am J Roentgenol 2014; 203(3):516–530. [PubMed: 25148154]
12. Argentieri EC, Koff MF, Breighner RE, Endo Y, Shah PH, Sneag DB. Diagnostic accuracy of zero-echo time MRI for the evaluation of cervical neural foraminal stenosis. Spine (Phila Pa 1976) 2018; 43(13):928–933. [PubMed: 29095415]
13. Breighner RE, Bogner EA, Lee SC, Koff MF, Potter HG. Evaluation of osseous morphology of the hip using zero echo time magnetic resonance imaging. Am J Sports Med 2019; 47(14):3460–3468. [PubMed: 31633993]
14. Breighner RE, Endo Y, Konin GP, Gulotta LV, Koff MF, Potter HG. Technical developments: zero echo time imaging of the shoulder: enhanced osseous detail by using MR imaging. Radiology 2018; 286(3):960–966. [PubMed: 29117482]
15. Cho SB, Baek HJ, Ryu KH, Choi BH, Moon JI, Kim TB, et al. Clinical feasibility of zero TE skull MRI in patients with head trauma in comparison with CT: a single-center study. American Journal of Neuroradiology 2019; 40(1):109–115. [PubMed: 30545839]
16. Lu A, Gorny KR, Ho M-L. Zero TE MRI for craniofacial bone imaging. American Journal of Neuroradiology 2019; 40(9):1562–1566. [PubMed: 31467238]

17. Patel KB, Eldeniz C, Skolnick GB, Jammalamadaka U, Commean PK, Goyal MS, et al. 3D pediatric cranial bone imaging using high-resolution MRI for visualizing cranial sutures: a pilot study. Journal of Neurosurgery: Pediatrics PED 2020; 26(3):311–317.
18. Chavhan GB, Babyn PS, Jankharia BG, Cheng H-LM, Shroff MM. Steady-state MR imaging sequences: physics, classification, and clinical applications. Radiographics 2008; 28(4):1147–1160. [PubMed: 18635634]
19. Link TM, Majumdar S, Grampp S, Guglielmi G, Kuijk Cv, Imhof H, et al. Imaging of trabecular bone structure in osteoporosis. Eur Radiol 1999; 9(9):1781–1788. [PubMed: 10602950]
20. Majumdar S, Genant HK, Grampp S, Newitt DC, Truong VH, Lin JC, et al. Correlation of trabecular bone structure with age, bone mineral density, and osteoporotic status: in vivo studies in the distal radius using high resolution magnetic resonance imaging. J Bone Miner Res 1997; 12(1):111–118. [PubMed: 9240733]
21. Yang X, Li Z, Cao Y, Xu Y, Wang H, Wen L, et al. Efficacy of magnetic resonance imaging with an SPGR sequence for the early evaluation of knee cartilage degeneration and the relationship between cartilage and other tissues. J Orthop Surg Res 2019; 14:152. [PubMed: 31126302]
22. Hsu H, Lachenbruch PA. Paired t test. Wiley StatsRef: Statistics Reference Online
23. Landis JR, Koch GG. The measurement of observer agreement for categorical data. Biometrics 1977; 33(1):159–174. [PubMed: 843571]
24. Virtanen P, Gommers R, Oliphant TE, Haberland M, Reddy T, Cournapeau D, et al. SciPy 1.0: fundamental algorithms for scientific computing in Python. Nature Methods 2020; 17:261–272. [PubMed: 32015543]
25. Sell CA, Masi JN, Burghardt A, Newitt D, Link TM, Majumdar S. Quantification of trabecular bone structure using magnetic resonance imaging at 3 Tesla—calibration studies using microcomputed tomography as a standard of reference. Calcif Tissue Int 2005; 76(5):355–364. [PubMed: 15868282]
26. Yoshioka H, Stevens K, Hargreaves BA, Steines D, Genovese M, Dillingham MF, et al. Magnetic resonance imaging of articular cartilage of the knee: comparison between fat-suppressed three-dimensional SPGR imaging, fat-suppressed FSE imaging, and fat-suppressed three-dimensional DEFT imaging, and correlation with arthroscopy. J Magn Reson Imaging 2004; 20(5):857864.
27. deMello RAF, Ma Y-J, Ashir A, Jerban S, Hoenecke H, Carl M, et al. Three-dimensional zero echo time magnetic resonance imaging versus 3-dimensional computed tomography for glenoid bone assessment. Arthroscopy 2020; 36(9):2391–2400. [PubMed: 32502712]
28. Lansdown DA, Pedoia V. Editorial commentary: can we evaluate glenoid bone with magnetic resonance imaging? Yes, if you have the right sequence. Arthroscopy 2020; 36(9):2401–2402. [PubMed: 32891242]
29. Weiger M, Wu M, Wurnig MC, Kenkel D, Boss A, Andreisek G, et al. ZTE imaging with long-T2 suppression. NMR Biomed 2015; 28(2):241–254.
30. Silva A, Pinto E, Sampaio R. Rotational alignment in patient-specific instrumentation in TKA: MRI or CT? Knee Surg Sports Traumatol Arthrosc 2016; 24(11):3648–3652. [PubMed: 25344804]
31. Jerban S, Chang DG, Ma Y, Jang H, Chang EY, Du J. An update in qualitative imaging of bone using ultrashort echo time magnetic resonance. Front Endocrinol 2020; 11:777.
32. Li Y, Li W, Xiong J, Xia J, Xie Y. Comparison of supervised and unsupervised deep learning methods for medical image synthesis between computed tomography and magnetic resonance images. Biomed Res Int 2020; 5193707. [PubMed: 33204701]
33. Florkow MC, Zijlstra F, Willemsen K, Maspero M, Berg CATvd, Kerkmeijer LGW, et al. Deep learning-based MR-to-CT synthesis: the influence of varying gradient echo-based MR images as input channels. Magn Reson Med 2020; 83(4):1429–1441. [PubMed: 31593328]
34. Geiger D, Bae WC, Statum S, Du J, Chung CB. Quantitative 3D ultrashort time-to-echo (UTE) MRI and micro-CT (μCT) evaluation of the temporomandibular joint (TMJ) condylar morphology. Skeletal Radiol 2014; 43(1):19–25. [PubMed: 24092237]
35. Deniz CM, Xiang S, Hallyburton RS, Welbeck A, Babb JS, Honig S, et al. Segmentation of the proximal femur from MR images using deep convolutional neural networks. Scientific Reports 2018; 8(1):16485. [PubMed: 30405145]

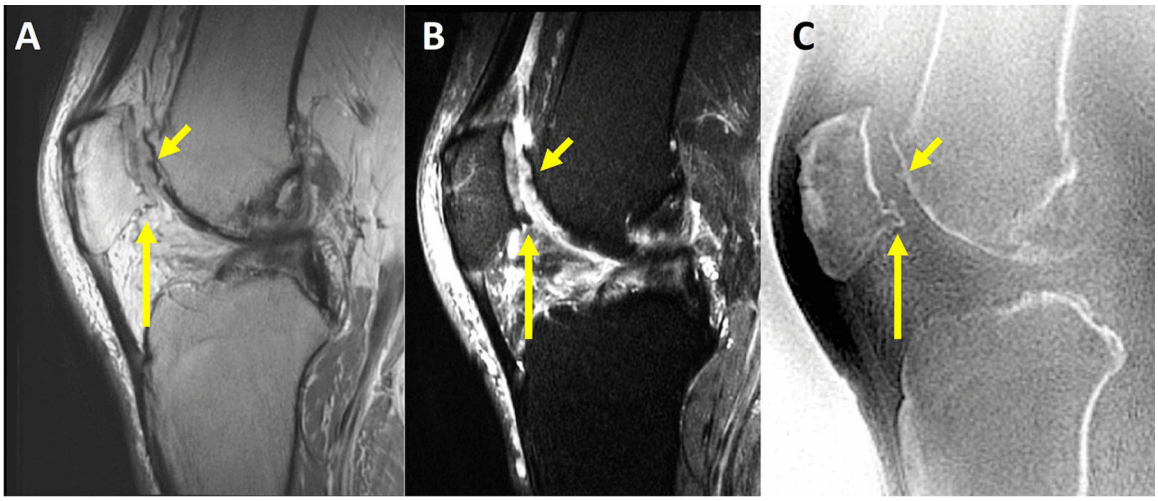

Fig. 1.

54-year-old man with left knee pain. PD = proton-density weighted (A), IwFS = intermediate-weighted fat saturated (B), and ZTE = zero echo time (C) sequences are shown. Complex morphology of inferior patellar osteophyte (large arrow) is better shown on ZTE sequences compared to PD and IwFS sequences. Small focal cartilage calcification (small arrow) is also better visualized on ZTE sequences, on the other sequences it only appears as signal inhomoegenity in the cartilage. Also note that overall bony contours are better shown on the ZTE sequences

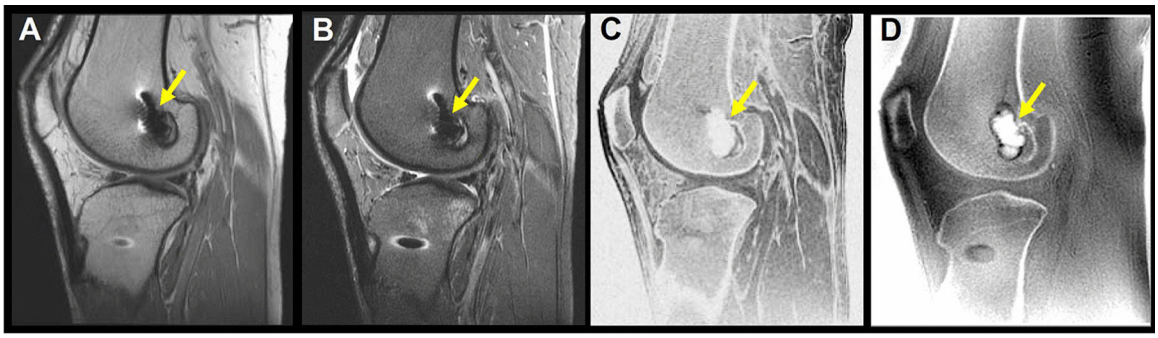

Fig. 2.

33-year-old woman with history of anterior cruciate ligament reconstruction presented with left knee pain after a fall. PD-weighted (A), IwFS-weighted (B), SPGR =spoiled gradient echo (C), and ZTE (D) sequences. Although performed at 3T both gradient echo (ZTE and SPGR) sequences showed the bony defect and may be useful in patients with hardware compared to standard sequences (IwFS and PD)

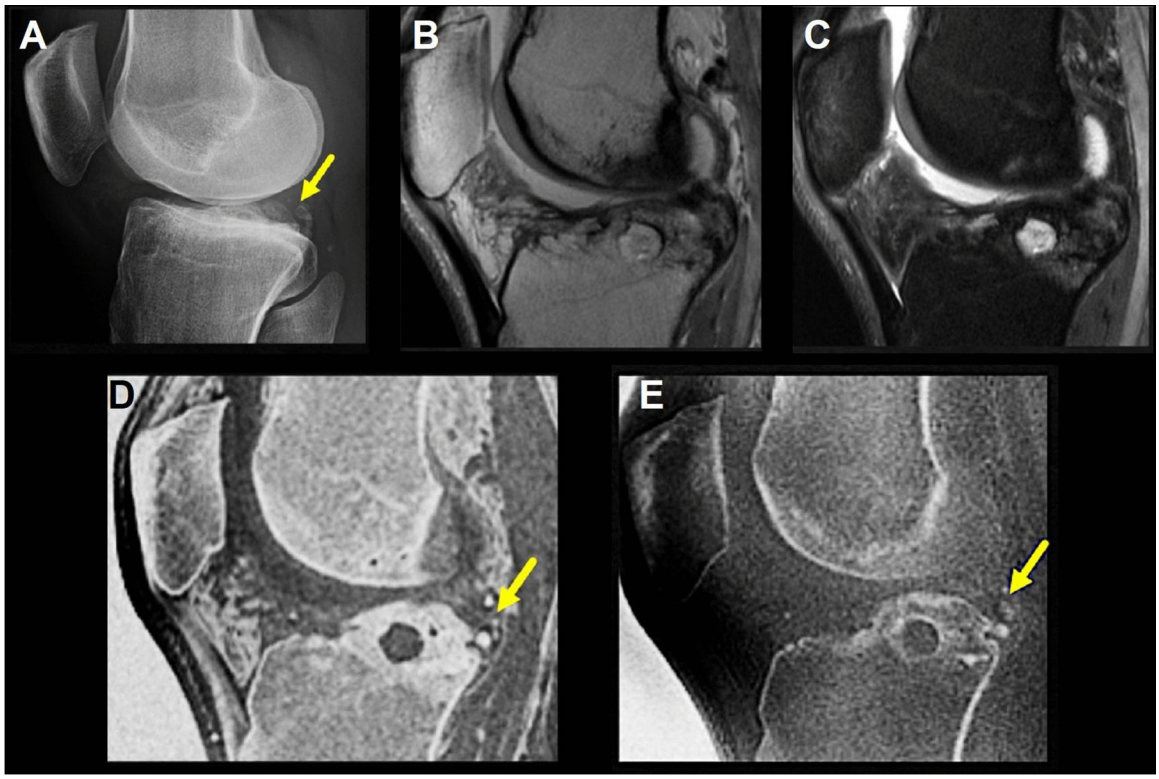

Fig. 3.

25-year-old man presented with left knee pain post-lateral meniscus transplant surgery. Radiograph (A), PD-weighted (B), IwFS-weighted (C), SPGR (D), and ZTE (E) sequences. While the posterior tibial calcification and osteochondral bodies (arrows) are well-characterized on the ZTE as well as SPGR sequences, they are not visualized on the PD and IwFS sequences. The radiograph shows multiple osseous densities (arrow in A), confirming the findings noted on ZTE and SPGR to be intra-articular bodies, ruling out image artifacts

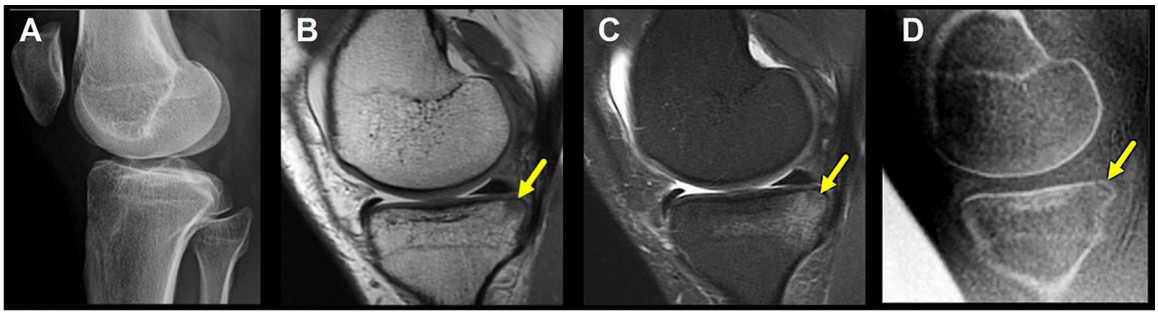

Fig. 4.

33-year-old woman presented with left knee pain after an injury while playing soccer. Radiograph (A), PD-weighted (B), IwFS-weighted (C), and ZTE (D) sequences. No fractures were visualized on the radiograph. MRI showed a complete tear of the anterior cruciate ligament and an impaction fracture of the posterior medial tibial plateau (arrow on the ZTE sequence). Although edema is visualized in the corresponding area of the PD and IwFS sequences, the fracture is not clearly visualized

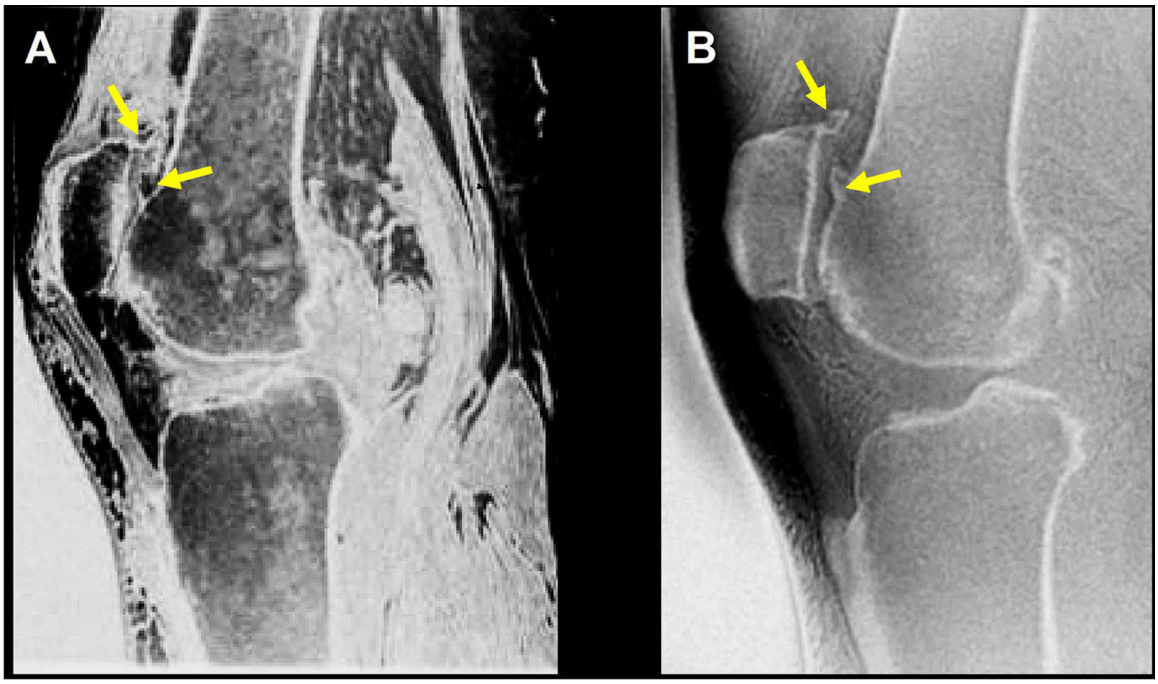

Fig. 5.

61-year-old woman presented with left knee pain and MRI shows degenerative changes with prominent osteophytes. SPGR (A) and ZTE (B) sequences. Superior femoro-patellar osteophytes (arrows) are well-characterized on the ZTE sequence (B) but are not well-visualized on the SPGR sequence (A)

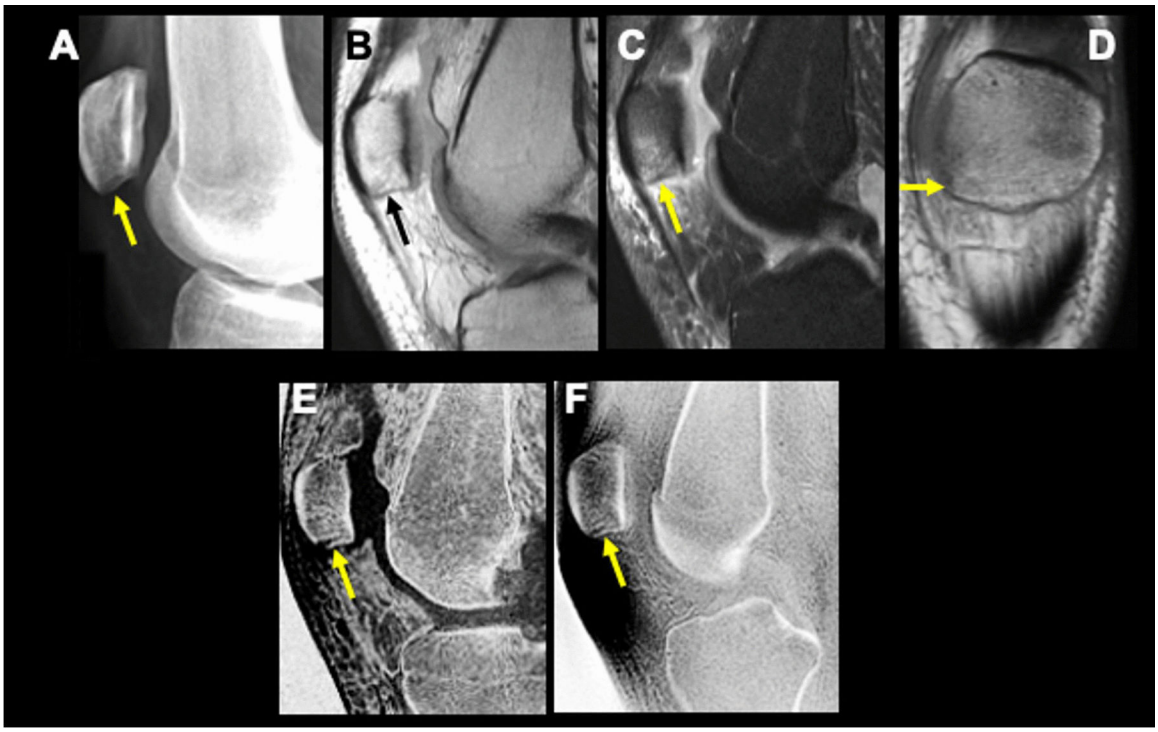

Fig. 6.

20-year-old woman presented with history of transient patellar dislocation after a fall from her bike. Radiograph (A), sagittal PD-weighted (B), sagittal IwFS-weighted (C), coronal T1-weighted (D), sagittal SPGR (E), and sagittal ZTE (F) sequences. Radiograph of the left knee does not visualize fractures or dislocations. MRI findings were consistent with transient dislocation with bone marrow edema pattern in standard MRI sequences at the inferior pole of the patella. The patellar fracture (arrows), however, is only seen on SPGR and ZTE sequences

Table 1

Acquisition parameters used in this study for ZTE, SPGR, and the clinical sequences

	Orientation	Fat saturation	Matrix (pixels)	FOV (cm)	Slice Thickness (mm)	Flip Angle	TE (ms)	TR (ms)
ZTE	Sagittal	No	256×128	14	2	1	0	0.5
SPGR	Sagittal	No	256×256	16	1.5	15	2	4.1
PD	Sagittal	No	224×224	13	4	90	20	2000
Iw FS	Sagittal	Yes	224×224	13	3	90	46	3200
Iw FS	Coronal	Yes	224×224	13	4	90	46	3200
T1	Coronal	No	224×224	13	4	90	46	600
Iw FS	Axial	Yes	224×224	13	4	90	46	3700

Table 2

Summary of image quality characteristics

n **= 299 (100 studies, 3 raters)** one reviewer assessed 99 cases, other two assessed 100**	**Image contrast**	**Image sharpness**	**Cortical bone depiction**	**Trabecular bone depiction**	**Image artifact**	**Image motion**
Unimpaired depiction of all structures (5)	143 47.7%	138 46.0%	149 49.7%	0 0.00%	217 72.3%	273 91.0%
Minimal impairment, preservation of all structural detail (4)	133 44.3%	158 45.2%	127 42.3%	106 35.3%	68 22.7%	25 8.3%
Impaired depiction of small areas (3)	20 6.7%	2 0.7%	22 7.3%	9 3.0%	12 4.0%	0 0.0%
Substantial obscuration of structures (2)	2 0.7%	0 0.0%	0 0.0%	181 60.3%	1 0.3%	0 0.0%
Complete obscuration of structures (1)	1 0.3%	1 0.3%	1 0.3%	3 1.0%	1 0.3%	1 0.3%

Table 3

Likert scores for assessing the reviewers' confidence in identifying osseous abnormalities using ZTE

	Fractures (*n* = 45)	**Osteophytosis (*n* = 104)**	**Subchondral cysts (*n* = 47)**	**Soft tissue calcifications (*n* = 26)**
Definitely certain (5)	32 71.1%	101 97.1%	40 85.1%	19 73.1%
Probably certain (4)	7 15.6%	3 2.9%	5 10.6%	5 19.2%
Not sure (3)	4 8.9%	0 0.0%	1 2.15%	2 7.7%
Probably not (2)	2 4.4%	0 0.0%	1 2.15%	0 0.0%
Definitely not (1)	0 0.0%	0 0.0%	0 0.0%	0 0.0%

For each abnormality, the total number of reviews (*n*) in which the osseous abnormality was noted is also reported

Table 4

Likert grades assessing the addition of ZTE to standard sequences for altering patient management, increasing diagnostic certainty, and providing additional value for the patient in cases where osseous findings were present ($n = 242$)

Osseous findings ($n = 242$)	ZTE alters patient management	ZTE increases diagnostic certainty	ZTE provides additional value for the patient
Definitely certain (5)	65 26.9%	85 35.1%	68 28.1%
Certain (4)	25 10.3%	75 30.9%	71 29.3%
Probable diagnosis (3)	40 16.5%	20 8.3%	30 12.4%
Probably not (2)	53 21.9%	24 10.0%	31 12.8%
Definitely not (1)	59 24.4%	38 15.7%	42 17.4%

Table 5

Likert grades assessing the addition of ZTE to standard sequences for altering patient management, increasing diagnostic certainty, and providing additional value for the patient in cases where no osseous findings were noted ($n = 58$)

No osseous findings ($n = 58$)	**ZTE alters patient management**	**ZTE increases diagnostic certainty**	**ZTE provides additional value for the patient**
Definitely certain (5)	2 3.4%	1 1.7%	1 1.7%
Certain (4)	5 8.6%	14 24.1%	8 13.7%
Probable diagnosis (3)	27 46.6%	9 15.6%	22 37.9%
Probably not (2)	10 17.2%	2 3.4%	6 10.4%
Definitely not (1)	14 24.2%	32 55.2%	21 36.3%

Table 6

Likert grades comparing the diagnostic confidence of ZTE vs SPGR sequences for assessing osseous structures and abnormalities as well as impact of soft tissues on the evaluation

n **= 171 (57 studies with both ZTE and SPGR × 3 reviewers)**	**Bony structures better seen on ZTE than on SPGR**	**Bony abnormalities better seen on ZTE than on SPGR**	**Soft tissue limits evaluation of osseous structures on SPGR**
Definitely certain	46 26.9%	57 33.3%	60 35.1%
Certain	45 26.3%	12 7.1%	47 27.5%
Probably certain	14 8.2%	17 9.9%	9 5.3%
Not certain	9 5.3%	66 38.6%	12 7.0%
Definitely not certain	57 33.3%	19 11.1%	43 25.1%

Table 7

Inter-reader reliability measured as pairwise agreements between radiologists using linearly weighted Cohen's kappa statistic for each category assessed on a 5-grade Likert scale

	Reader 1 vs reader 2	**Reader 2 vs reader 3**	**Reader 3 vs reader 1**
Confidence in using ZTE for assessing osteophytosis	*0.41*	*0.52*	*0.58*
Confidence in using ZTE for assessing subchondral cysts	*0.43*	*0.55*	*0.58*
Bony structures better on ZTE vs SPGR	*0.57*	*0.28*	*0.31*
Bony abnormalities better on ZTE vs SPGR	*0.63*	*0.28*	*0.27*